

Conductive Nature of Grain Boundaries in Nanocrystalline Stabilized Bi₂O₃ Thin-Film Electrolyte

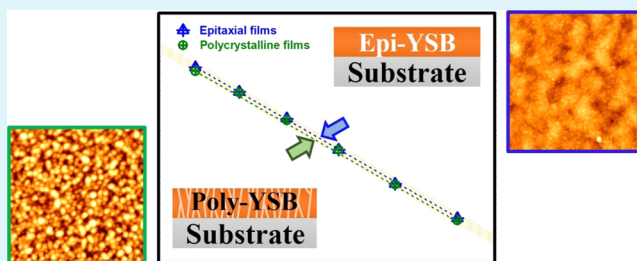
Seung Jin Jeong,[†] No Woo Kwak,[†] Pilgyu Byeon,[‡] Sung-Yoon Chung,[‡] and WooChul Jung^{*,†}

[†]Department of Materials Science and Engineering and [‡]Graduate School of EEWS, Korea Advanced Institute of Science and Technology (KAIST), Daejeon 34141, Korea

Supporting Information

ABSTRACT: Stabilized Bi₂O₃ has gained a considerable amount of attention as a solid electrolyte material for low-temperature solid oxide fuel cells due to its superior oxygen-ion conductivity at the temperature of relevance (≤ 500 °C). Despite many research efforts to measure the transport properties of stabilized Bi₂O₃, the effects of grain boundaries on the electrical conductivity have rarely been reported and their results are even controversial. Here, we attempt quantitatively to assess the grain boundary contribution out of the total ionic conductivity at elevated temperatures (350–500 °C) by fabricating epitaxial and nano-polycrystalline thin films of yttrium-stabilized Bi₂O₃. Surprisingly, both epitaxial and polycrystalline films show nearly identical levels of ionic conductivity, as measured by alternating current impedance spectroscopy and this is the case despite the fact that the polyfilm possesses nanosized columnar grains and thus an extremely high density of the grain boundaries. The highly conductive nature of grain boundaries in stabilized Bi₂O₃ is discussed in terms of the clean and chemically uniform grain boundary without segregates, and the implications for device application are suggested.

KEYWORDS: stabilized Bi₂O₃, solid electrolyte, grain boundary, thin film, electrical conductivity



INTRODUCTION

Solid electrolytes with high oxygen-ion conductivity are of significant interest for many applications, such as solid oxide fuel cells, gas sensors, and permeation membranes. Over the past several decades, numerous studies have been conducted on the effect of grain boundaries on the process of increasing the ionic conductivity of solid electrolytes.^{1–4} For materials with a fluorite structure (i.e., yttria-stabilized zirconia (YSZ) or acceptor-doped ceria), grain boundaries are known to interfere with the transport of oxygen ions, particularly when the oxygen ions move across them. The loss of symmetry at the grain boundary relative to the bulk induces the segregation of dopants or impurities to constrict the migration path of oxygen ions.^{5–7} Furthermore, the space-charge region formed around intrinsically charged grain boundaries often inhibits the movement of oxygen ions.^{8–10} Given that nanocrystalline thin or thick films have been investigated in relation to lowering the operating temperature of solid electrolytes to less than 500 °C,^{11–13} more rigorous and quantitative assessments are necessary to determine how the oxygen-ion transport characteristics are affected by the numerous interfaces formed from a high density of nanograins.

Stabilized Bi₂O₃ has attracted much attention as a promising electrolyte because it has remarkably high oxygen-ion conductivity even at relatively reduced temperatures. This high conductivity is attributed to the inherently large number of oxygen vacancies (one out of four oxygen sites) and to the high oxygen-ion mobility caused by the high polarizability of Bi³⁺

with its lone-pair 6s² electrons in addition to the ability of Bi³⁺ to accommodate highly disordered surroundings.¹⁴ However, unlike other electrolyte materials, the grain boundary effect of stabilized Bi₂O₃ on the transport properties has rarely been reported and thus remains unclear.^{15–22} This is mainly due to the remarkably conductive nature of the grain boundaries of Bi₂O₃ and the technical difficulties involved in analyzing the grain boundary properties precisely. A common means of determining the contribution of the grain boundaries to the overall conductivity of a solid electrolyte is to make a dense polycrystalline pellet with metallic electrodes on both sides and analyze the impedance response with the frequency. According to the literature, in the case of stabilized Bi₂O₃, however, the impedance spectra corresponding to the bulk interior and grain boundaries were not distinguished.^{15,17,21,22} Considering the relatively large interfacial capacitance of the grain boundary itself, this indicates that the specific conductivity of the grain boundary is too high to be detected. Moreover, the typical analytical method mentioned above makes it difficult to separate the conductivity of the grain boundary from the bulk as the temperature rises (usually above 350 °C) due to the limitations of the frequency range of the measuring instrument.²³ Therefore, even if one succeeds in analyzing the low-temperature conductivity of grain boundaries, this value is likely

Received: November 6, 2017

Accepted: January 25, 2018

Published: January 25, 2018

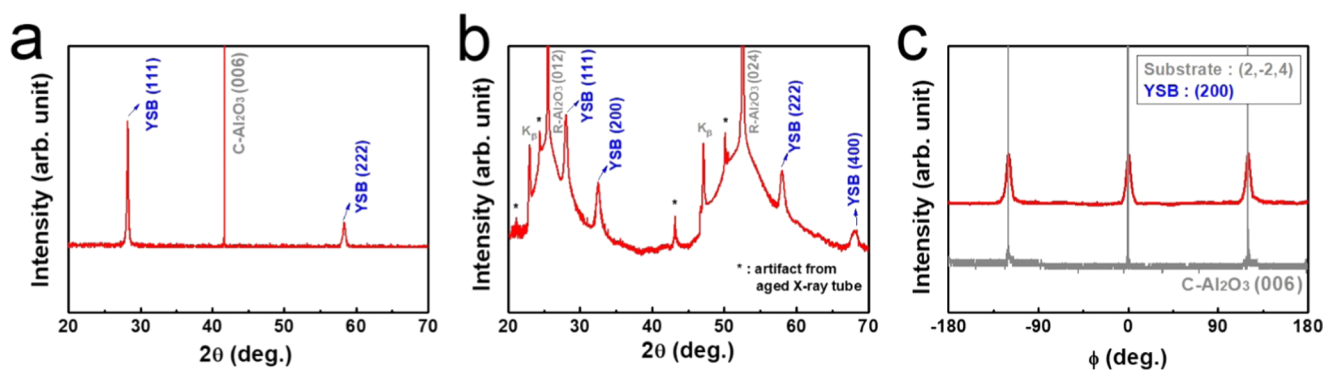


Figure 1. X-ray diffraction data for the Y-stabilized Bi_2O_3 (YSB) thin films grown on single-crystal Al_2O_3 substrates with different orientations. Out-of-plane diffraction patterns (2θ scan) of the films (a) on C- Al_2O_3 (0001) and (b) on R- Al_2O_3 (1102). (c) In-plane diffraction patterns (ϕ scan) of the C- Al_2O_3 substrate and the YSB films (X-ray diffraction data for the different thicknesses are plotted in Figure S1).

to come from a phase with lower symmetry rather than a cubic fluorite structure (δ -phase) because Bi_2O_3 undergoes a variety of phase transitions at low temperatures.^{24–26} Serious errors in extrapolating large temperature differences also cannot be ignored. Therefore, to resolve these issues, new techniques which accurately analyze the bulk and grain boundary transport properties of samples while maintaining the δ -phase at the desired elevated temperatures (e.g., 350–500 °C) are needed.

In this study, we fabricated both epitaxial and polycrystalline thin films of Y-stabilized Bi_2O_3 (YSB) on two different single-crystal substrates (C-plane Al_2O_3 (0001) and R-plane Al_2O_3 (1102)) and measured their in-plane ionic conductivity values over a wide range of oxygen partial pressures ($p\text{O}_2$) and temperatures. The remarkably high grain boundary density of the polyfilms with vertically oriented, nanosized columnar grains is expected to enhance the contribution of the grain boundaries significantly, relative to the total conduction. Furthermore, the use of substrate-constrained thin-film samples inhibits further phase transitions, allowing us to measure the conductivity of the targeted cubic fluorite structure. Here, we observed that the ionic conductivity of the grain boundaries, especially when oxygen ions migrate across the grain boundaries, was too high to detect any difference in conduction characteristics between epitaxial and nano-polycrystalline YSB films within a reasonable degree of measurement error. This extremely highly conductive behavior of stabilized Bi_2O_3 grain boundaries is discussed in regard to the microstructure and dopant/impurity segregation.

EXPERIMENTAL METHODS

Sample Preparation. $\text{Y}_{0.25}\text{Bi}_{0.75}\text{O}_3$ (25 mol % Y_2O_3 -stabilized Bi_2O_3 , YSB) thin films were prepared by means of pulsed laser deposition (PLD) from oxide targets of the respective materials. The targets were prepared by solid-state synthesis of powder mixtures: the Bi_2O_3 (99.9995%, Alfa Aesar) and Y_2O_3 (99.99%, Alfa Aesar) powders were used. The powder mixtures were zirconia ball-milled with a high-purity ethanol media in a polyethylene bottle for 24 h and dried in air for 24 h. The mixed powders were then calcined in air at 800 °C for 5 h and isostatically cold-pressed at 200 MPa, followed by sintering under air at 890 °C for 16 h to create a PLD target. A flat cylindrical ceramic target having a diameter of 2.54 cm (1 in.) and a thickness of 1 cm was used for the film deposition. The distance between the target and substrate was 6 cm. Thin films with thickness ranging from 60 to 450 nm were prepared by means of PLD on single-crystalline sapphire substrates with different orientations of C-plane Al_2O_3 (0001) and R-plane Al_2O_3 (1102) substrates, with a size of $10 \times 10 \times 0.5 \text{ mm}^3$ (MTI). The PLD system was operated with a KrF excimer laser, emitting at 248 nm (Coherent COMPex 205), at pulsed laser energy

of 300 mJ and a laser repetition rate of 5 Hz. The substrates were heated to 700 °C during deposition, and O_2 working pressure was kept at 10 mTorr. After the deposition process, all of the samples were annealed at 700 °C, 1 Torr of O_2 working pressure for 30 min to ensure that they were fully oxidized.

Physical Characterization. X-ray diffraction (XRD) measurements were conducted to investigate the crystal structures of deposited YSB films using a Bragg-Brentano diffractometer (Rigaku Ultima IV, Tokyo, Japan, Cu $K\alpha$ wavelength ($\lambda = 1.541 \text{ \AA}$)). In-plane reflections through high-resolution X-ray diffraction measurements were taken for precise analysis of the growth structure and crystallinity of the deposited films using a diffractometer (X'Pert-PRO MRD, PANalytical) operated at 45 kV and 40 mA with a fixed Cu anode.

The grain size, morphology, and surface roughness of the thin films were characterized by an atomic force microscope (AFM) analysis using a Bruker (Innova) device in tapping mode. The cross sections of the resulting films were examined using a (S-4800, Hitachi) scanning electron microscope. Bright-field transmission electron microscopy (TEM) and Z-contrast high-angle annular dark-field scanning transmission electron microscopy (HAADF-STEM) images were taken with a transmission electron microscope (Titan cubed G2 60-300, FEI) at 300 kV, with a spherical aberration (Cs) corrector (CEOS GmbH). Chemical line scan with energy-dispersive spectrometry (EDS) was carried out in a transmission electron microscope (Talos F200x, FEI) operated at 200 kV. A four windowless silicon drift detectors EDS system (Super X) was used as EDS detector.

In-Plane Conductivity Measurement. In-plane conductivity measurements were undertaken using alternating current impedance spectroscopy (ACIS, VSP-300, Biologic) at frequencies ranging from 5 MHz to 1 Hz, with AC amplitude of 200 mV. An AC amplitude of 200 mV was used after confirming that this voltage lies within the linear regime of the sample's current–voltage response.^{10,17,27} Two platinum electrodes (130 nm in thickness) were sputtered onto the films using a metal shadow mask. The spacing between the two Pt electrodes was fixed at 1 mm, which is much larger than the thickness of the YSB films (60–430 nm), to prevent the constriction effect. The measurements were carried out at temperatures of 350–500 °C and $p\text{O}_2$ of 2×10^{-4} –1 atm, in which the $p\text{O}_2$ values were controlled by mixing oxygen and argon gases in a tube furnace. Each sample was considered to reach equilibrium at a given temperature and $p\text{O}_2$, after confirming that the changes in the impedance spectra lie within 2% error between sequential measurements separated in time by 10 min.

RESULTS AND DISCUSSION

Physical Characterization of the YSB Films. Figure 1 shows the X-ray diffraction patterns of YSB thin films grown on C-plane Al_2O_3 (0001) and R-plane Al_2O_3 (1102) single-crystal substrates. The out-of-plane results (ω - 2θ scan) indicate that films with high crystallinity are successfully obtained with a cubic fluorite structure (δ -phase) without any amorphous or

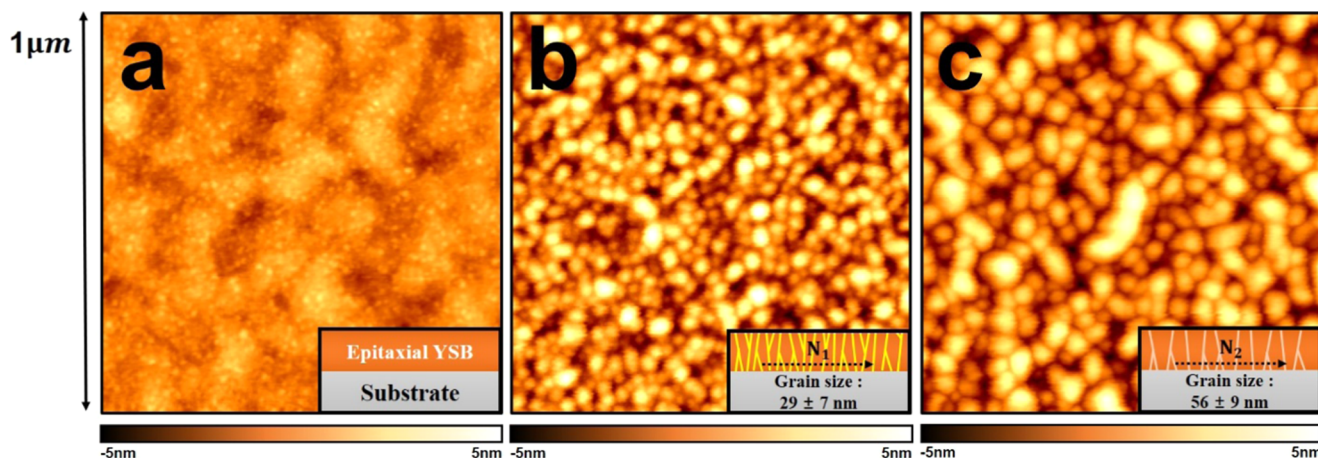


Figure 2. AFM micrographs of (a) an epitaxial Y-stabilized Bi_2O_3 thin film with the thickness of 182 nm on C- Al_2O_3 (0001) and (b, c) columnar films with the thickness of (b) 135 nm and (c) 430 nm on R- Al_2O_3 ($1\bar{1}02$).

secondary phase. Indeed, the film on the C-plane substrate shows only the (111) peak, indicative of coherent film growth, whereas several peaks corresponding to both the (111) and (200) peaks are observed from those on the R-plane substrate. In-plane diffraction patterns in Figure 1b provide further evidence of the epitaxial growth of YSB films. Unlike the polycrystalline film without any peaks in the in-plane φ -scan results, the film on the C-plane shows sharp in-plane peaks with a 3-fold rotational symmetry of 120° , which confirms the good alignment registry between the film and the substrate. Similarly, the deposition of epitaxial stabilized Bi_2O_3 (111) film on C- Al_2O_3 (0001) was also reported elsewhere.²⁷

AFM images of the surfaces of the YSB films are shown in Figure 2. The lateral dimensions all samples span $1 \mu\text{m}$; the vertical dimension in the image is indicated on the z-axis scale as 10 nm. Figure 2a shows the surface of the epitaxial YSB thin film, which is too flat to confirm the presence of grain boundaries. In contrast, in the polycrystalline film shown in Figure 2b,c, nanoscale grains can be clearly identified; here, as the thickness of the film increases, the grain size increases, and thus the density of the grain boundary decreases. For example, thin films with a thickness of 135 ± 7 nm have a grain size of 29 ± 7 nm, whereas with an increase in the thickness at 430 ± 3 nm, the grain size increases to 56 ± 9 nm. See Figure S2 for more information on measuring the average grain size and grain boundary density. It is noteworthy that the root mean square surface roughness remains less than 2 nm in all samples. Such flat and dense layers cannot be realized with the oxide pellets used in a conventional bulk ceramic process.

The chemical compositions of PLD targets and the deposited films were also investigated via inductively coupled plasma mass spectrometry. Considering the loss of bismuth in the high-temperature and high-vacuum conditions of the PLD process,^{27,28} we analyzed the composition of the thin films using targets with three different Y/Bi cation ratios (Figure S3). As a result, it was confirmed that the PLD target with 18% of Y cations could produce the YSB 25 (25% of Y) thin film used in this study.

Impedance Spectra of YSB Films. The oxygen-ion conductivity of YSB thin films was measured at 350–500 °C via ACIS. Figure 3 shows the typical impedance spectra obtained for both epitaxial and columnar films. The impedance response, plotted in Nyquist form, always exhibits a nearly ideal semicircle for all samples; thus, the semicircle is modeled using

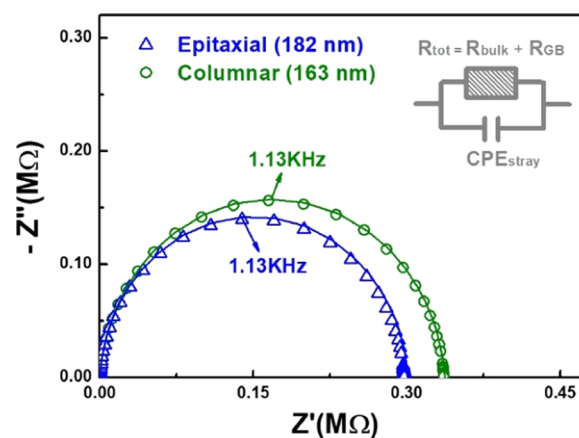


Figure 3. Typical impedance spectra of epitaxial (triangle) and columnar (circle) Y-stabilized Bi_2O_3 thin films with a similar thickness measured at 500 °C and $p\text{O}_2 = 0.21$ atm.

a RQ subcircuit, where Q is a constant-phase element with impedance Z_Q equal to $1/Q(i\omega)^n$, n is a constant, and ω is the frequency. Consistent with the near-ideal shape of the impedance response, the fitted n value was found to fall within the range of 0.94–0.96. Several features of the resistive part of the impedance are consistent, with the source being the ionic conduction of the YSB films. This includes the resistance value of the YSB films, which linearly decreases as the film thickness increases (see Figure S4), and the fact that the resistance value remains constant despite the change of the oxygen partial pressure between 2×10^{-4} and 1 atm (inset graph in Figure 4).

Furthermore, the magnitude of conductivity, calculated on the basis of the film thickness, the distance between the Pt electrodes, and the measured resistance values, was in good agreement with the literature data^{19,25} for the ionic conductivity of YSB (Figure 4). One can thus evidently conclude that the impedance feature should be attributed to the oxygen-ion conduction of YSB film. Note that the electronic leakage currents through the insulating substrates can be neglected, as the measured conductivity of the bare substrates is several orders of magnitude lower than that of the YSB thin film (Figure S5).

Turning to the capacitive part of the impedance, the measured values show a very large capacitance ($\sim 10^{-10}$ F) and are constant regardless of the thickness of the deposited

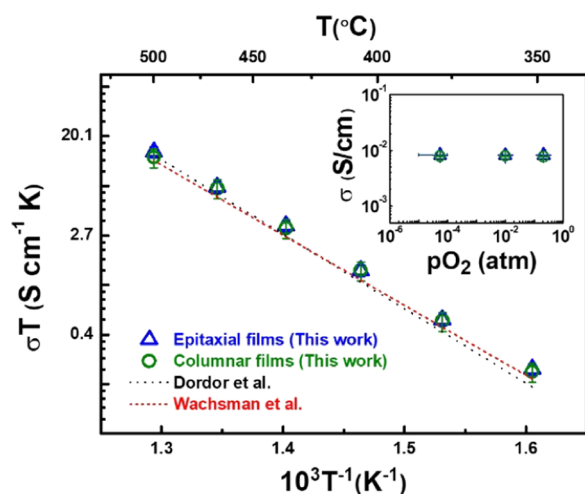


Figure 4. Arrhenius plot of the electrical conductivity of epitaxial (triangle) and columnar (circle) Y-stabilized Bi_2O_3 thin films compared with works taken from Dordor¹⁹ and Wachsman.²⁵ Double-logarithmic plots (insets) of the electrical conductivity of the films vs $p\text{O}_2$ at 500 °C, showing the films are fully oxygen-ion conductors.

films. These observations were frequently reported when measuring the electrical conductivity of a thin film on a dielectric substrate, and they are attributable to the substrate stray capacitance, whose value is several orders of magnitude higher than the capacitance levels of the bulk and grain boundary of the YSB films. Accordingly, due to the substrate capacitance connected in parallel with the YSB capacitance, the impedance spectra corresponding to the bulk interior and grain boundaries cannot be distinguished and only the sum of both resistive contributions was measured in this study.

The measured oxygen-ion conductivity values for both epitaxial and polycrystalline films are shown in Figure 4. The error bars shown are average values measured for thin films with three different thicknesses. Because the polyfilm has both bulk and grain boundary effects on the impedance, the resistance value is expected to be larger than that of the epifilm. However, surprisingly, we could not find any significant difference in the conductivity between the epitaxial and columnar films within the error range of 11%. This is the case despite the fact that the polycrystalline samples have very small grain sizes (29–56 nm) and thus very large grain boundary densities (18–33 ($1/\mu\text{m}$)). The activation energy corresponding to the oxygen-ion conduction was constant in all samples, regardless of the presence or absence of grain boundaries, which is also consistent with the values reported (1.25 eV) in the literature, i.e., 1.22 eV for the epitaxial and 1.21 eV for the polycrystalline types (Table 1). Previously, we assessed the specific grain boundary conductivity of acceptor-doped CeO_2 using thin-film samples akin to those used in this study. There, the difference in the resistance between epitaxial

Table 1. E_a (eV) and Conductivity (σ (S/cm)) of Epitaxial and Columnar Y-stabilized Bi_2O_3 thin films^a

sample	E_a (eV)	σ (S/cm)
epitaxial	1.22 ± 0.11	0.019 ± 0.002
columnar	1.21 ± 0.12	0.017 ± 0.002

^aThe conductivity values were obtained at 500 °C and $p\text{O}_2 = 0.21$ atm.

and nano-polycrystalline ceria films was more than double and the activation energy values between the two films were remarkably different (i.e., 0.75 and 1.23 eV for the bulk and grain boundary of Sm-doped CeO_2 , respectively).¹⁰ One can therefore conclude that the grain boundary of YSB is notably conductive to oxygen ions; these observations contradict those of the commonly used YSZ or doped ceria electrolytes, where the grain boundary acts as a blocker to prevent oxygen migration.^{29–31}

By the way, it needs to be noted that there are two possible pathways in which oxygen ions migrate at grain boundaries in a polycrystalline electrolyte: (1) across the grain boundary and (2) along the grain boundary. In this study, owing to the large substrate capacitance, only one impedance semicircle was observed in the YSB thin-film samples; hence, the conductivity values corresponding to those pathways could not be separated. However, we are certain that our observations correspond to the process of oxygen ions crossing the grain boundaries for the following two reasons. First, in the path along the grain boundaries, oxygen ions must travel a much longer distance through a much narrower section than a path across the grain boundaries. Specifically, the columnar thin-film structure greatly limits the number of paths along the grain boundaries (see Figure S6). Second, the conduction characteristics of the both epitaxial and columnar films cannot be precisely matched if the overall conductivity of the columnar film is predominantly determined by oxygen ions along the grain boundaries, as oxygen ions moving along the grain boundaries do not pass through the bulk grain interiors, implying that there is no reason for the bulk properties of the epitaxial film to appear in the polycrystalline film.

Atomic-Scale Analysis of the YSB Grain Boundary. To understand the excellent grain boundary conductivity of the YSB thin film, we attempted an atomic-level analysis using TEM. Figure 5 shows a STEM Z-contrast image of the grain boundaries of the columnar-grown YSB film on a $\text{R-Al}_2\text{O}_3$ substrate. As shown in the enlarged magnification, a very clean grain boundary between two adjacent grains is observed without any amorphous layer or secondary/impurity phase. The EDS line scan results for the thin-film cross-section exhibit no local compositional changes of the Bi and Y contents near grain boundaries, indicating that Y does not selectively accumulate at the grain boundaries. More information on the compositional distribution of the YSB film is provided in Figure S7. These observations are quite different from those with other fluorite electrolytes (i.e., YSZ or acceptor-doped ceria), where dopants such as Y and Gd are easily segregated at the grain boundaries.^{1,2,6,30–32} Note that the powder synthesis and sintering temperature of YSB is in the range of 800–890 °C, and the film deposition temperature of 700 °C used in this study is sufficiently high for local cation migration, considering the decomposition temperature (or melting temperature) of the material. Therefore, the uniform composition distribution around the grain boundaries observed in this study is not due to low deposition temperature.

There are two main reasons for the inhibition of oxygen-ion transport across the grain boundary in the oxide electrolyte.^{6,32} The first is the formation of space-charge regions, where oxygen vacancies are deficient around the grain boundary due to a grain boundary core with a relatively excess positive charge. The second is the selective segregation of the dopant or impurity into the grain boundary and the formation of insulating phases, which physically constricts the oxygen-ion currents by blocking

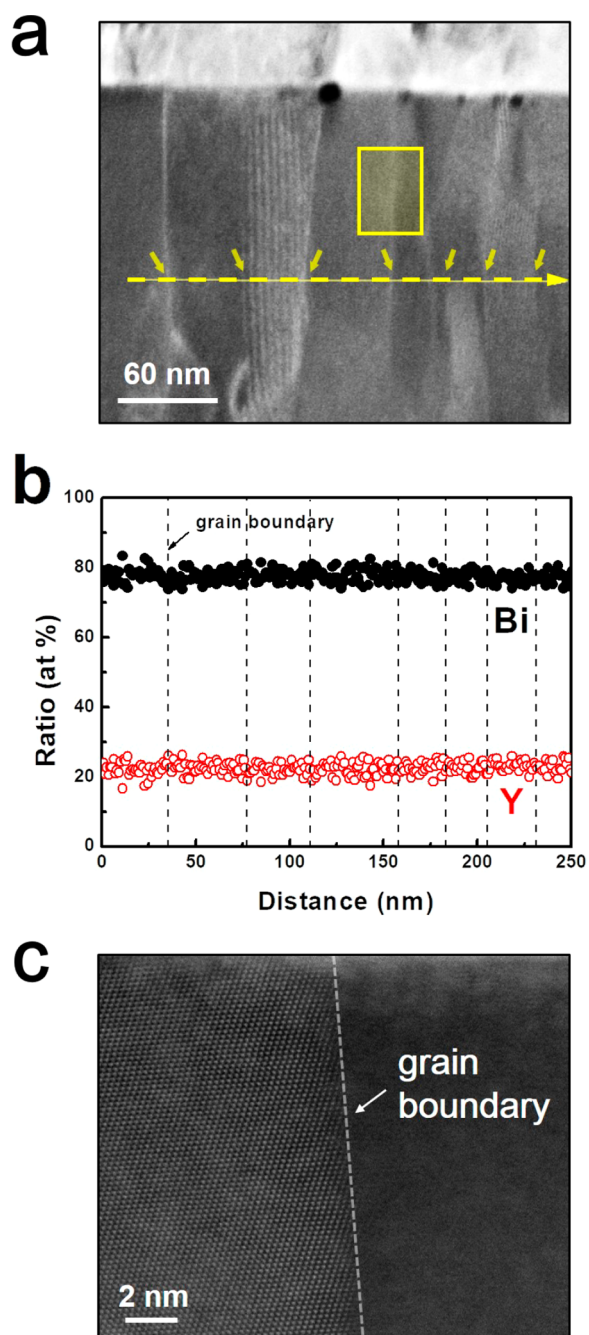


Figure 5. Cross-sectional microstructure and atomic structure of adjacent grains and grain boundary revealed by HAADF-STEM images. (a) Cross-sectional image shows distinguishable columnar grain boundaries in the Y-stabilized Bi_2O_3 film. (b) EDS compositional profile of Y and Bi elements measured across several grains and grain boundaries. (c) The magnified image of yellow rectangle in the above side reveals the crystal–crystal interface without any amorphous intergranular phases.

migration paths. Given that YSB has a very high carrier (oxygen vacancy) concentration of 25%, the space-charge effect will be negligible. Thus, in this study, it is suggested that the presence of a clean and chemically uniform grain boundary, as confirmed by the TEM analysis, would result in surprisingly high specific grain boundary conductivity.

The solute segregation phenomenon at the grain boundary of a solid solution is usually explained by two causes: elastic and

electrostatic effects. If the difference in radius between a dopant and a host atom is large, the host atoms cannot fully cope with the strain due to the introduction of an excessive amount of dopant; thus, the dopants will more likely diffuse from the grains into the grain boundaries, which have a relatively open structure and a low strain field.^{33,34} Arora et al. calculated the average segregation energy in several types of fluorite structures (CeO_2 , ZrO_2 , and UO_2) as a function of the dopant radii and reported that the weakest segregation tendencies appeared when using dopants with ionic radii most similar to that of the host cation.³⁵ However, in this study, the size mismatch between Y^{3+} and Bi^{3+} cations ($r[\text{Y}^{3+}] = 102 \text{ pm}$; $r[\text{Bi}^{3+}] = 117 \text{ pm}$),³⁶ is only 13%; thus, the driving force to release Y^{3+} to the grain boundary is not likely to be sufficient. Moreover, the high polarizability of Bi^{3+} with its lone-pair $6s^2$ electrons makes it possible to accommodate the local strain fully around Y^{3+} . Next, selective solute segregation can occur when the solute cations are effectively charged in the lattice compared to that in the host.^{9,37,38} However, in this study, the electrostatic effect is expected to be insignificant because Y^{3+} is an isovalent dopant, which is substituted in the Bi^{3+} cation site. Above all, unlike zirconia or ceria electrolytes, where the segregation of the aliovalent dopants and subsequent phase separation occur, Y-stabilized Bi_2O_3 can maintain a more homogeneous local composition, which plays an important role in the conductive nature of grain boundaries. However, it should be noted that Bi_2O_3 reacts easily with impurities such as silica and alumina, which come from conventional high-temperature ceramic processes, with high solubility.³⁹ Therefore, the development of fabrication techniques to prevent contamination, such as the vacuum deposition process used in this study, can maximize the advantages of oxygen-ion conduction characteristics at Bi_2O_3 grain boundaries.

SUMMARY

In this study, we confirmed the high oxygen-ion conductivity of the YSB grain boundary through highly controlled sample preparation and high-resolution analysis steps with a high level of accuracy. Both epitaxial and polycrystalline YSB films were grown via PLD on single-crystal Al_2O_3 substrates with different orientations, in this case the C-plane (0001) and R-plane (1 $\bar{1}$ 02) types. The ACIS results showed nearly identical levels of ionic conductivity in both the epitaxial and polycrystalline films, indicating that the extremely high grain boundary densities do not significantly affect the oxygen-ion conduction. These observations suggest that stabilized Bi_2O_3 is a powerful thin-film electrolyte capable of producing high-performance outcomes without any deleterious effects, even when used with nanoscale thin films having extremely high density levels of the grain boundaries.

ASSOCIATED CONTENT

Supporting Information

The Supporting Information is available free of charge on the ACS Publications website at DOI: 10.1021/acsami.7b16875.

Additional physical, chemical, and electrical characterizations on Y-stabilized Bi_2O_3 thin films and targets (Figures S1, S3–S5, and S7); illustrations and schematics applied to support our explanations (Figures S2 and S6) (PDF)

AUTHOR INFORMATION

Corresponding Author

*E-mail: wujung@kaist.ac.kr

ORCID

Seung Jin Jeong: 0000-0001-6125-6833

WooChul Jung: 0000-0001-5266-3795

Notes

The authors declare no competing financial interest.

ACKNOWLEDGMENTS

This work was supported by the Korea Institute of Energy Technology Evaluation and Planning (KETEP) and the Ministry of Trade, Industry & Energy (MOTIE) of the Republic of Korea (No. 20174030201590) and additionally supported by Nano Material Technology Development Program through the National Research Foundation of Korea (NRF) funded by the Ministry of Science, ICT and Future Planning (NRF-2017M3A7B4049547). The authors thank Hyung Bin Bae and Jin Seok Choi at KAIST Analysis Center for their support and assistance during the TEM analysis.

REFERENCES

- (1) Lin, Y.; Fang, S.; Su, D.; Brinkman, K. S.; Chen, F. Enhancing grain boundary ionic conductivity in mixed ionic-electronic conductors. *Nat. Commun.* **2015**, *6*, No. 6824.
- (2) Mahato, N.; Banerjee, A.; Gupta, A.; Omar, S.; Balani, K. Progress in material selection for solid oxide fuel cell technology: A review. *Prog. Mater. Sci.* **2015**, *72*, 141–337.
- (3) Mills, E. M.; Kleine-Boymann, M.; Janek, J.; Yang, H.; Browning, N. D.; Takamura, Y.; Kim, S. YSZ thin films with minimized grain boundary resistivity. *Phys. Chem. Chem. Phys.* **2016**, *18*, 10486–10491.
- (4) Jiang, S. H.; Wagner, J. B. A Theoretical-Model for Composite Electrolytes .1. Space-Charge Layer as a Cause for Charge-Carrier Enhancement. *J. Phys. Chem. Solids* **1995**, *56*, 1101–1111.
- (5) Aoki, M.; Chiang, Y. M.; Kosacki, I.; Lee, I. J. R.; Tuller, H.; Liu, Y. P. Solute segregation and grain-boundary impedance in high-purity stabilized zirconia. *J. Am. Ceram. Soc.* **1996**, *79*, 1169–1180.
- (6) Guo, X.; Waser, R. Electrical properties of the grain boundaries of oxygen ion conductors: Acceptor-doped zirconia and ceria. *Prog. Mater. Sci.* **2006**, *51*, 151–210.
- (7) Kingery, W. D. The Chemistry of Ceramic Grain-Boundaries. *Pure Appl. Chem.* **1984**, *56*, 1703–1714.
- (8) Kim, S.; Fleig, J.; Maier, J. Space charge conduction: Simple analytical solutions for ionic and mixed conductors and application to nanocrystalline ceria. *Phys. Chem. Chem. Phys.* **2003**, *5*, 2268–2273.
- (9) Wang, Q.; Lian, G.; Dickey, E. C. Grain boundary segregation in yttrium-doped polycrystalline TiO₂. *Acta Mater.* **2004**, *52*, 809–820.
- (10) Kwak, N. W.; Jung, W. Analysis of the grain boundary conductivity of singly and doubly doped CeO₂ thin films at elevated temperature. *Acta Mater.* **2016**, *108*, 271–278.
- (11) Figueiredo, F. M. L.; Marques, F. M. B. Electrolytes for solid oxide fuel cells. *Wiley Interdiscip. Rev.: Energy Environ.* **2013**, *2*, 52–72.
- (12) Omata, T.; Goto, Y.; Otsuka-Yao-Matsuo, S. Nanocrystals of zirconia- and ceria-based solid electrolytes: Syntheses and properties. *Sci. Technol. Adv. Mater.* **2007**, *8*, 524–530.
- (13) Singh, B.; Ghosh, S.; Aich, S.; Roy, B. Low temperature solid oxide electrolytes (LT-SOE): A review. *J. Power Sources* **2017**, *339*, 103–135.
- (14) Wang, S.-F.; Hsu, Y.-F.; Tsai, W.-C.; Lu, H.-C. The phase stability and electrical conductivity of Bi₂O₃ ceramics stabilized by Co-dopants. *J. Power Sources* **2012**, *218*, 106–112.
- (15) Lee, Y. J.; Park, C. O.; Baek, H. D.; Hwang, J. S. Grain boundary effect in (Bi₂O₃)_{0.75}(WO₃)_{0.25} and (Bi₂O₃)_{0.7}(SrO)_{0.3} solid electrolytes. *Solid State Ionics* **1995**, *76*, 1–4.
- (16) Duran, P.; Jurado, J. R.; Moure, C.; Valverde, N.; Steele, B. C. H. High Oxygen ion Conduction in some Bi₂O₃-Y₂O₃(Er₂O₃) Solid-Solutions. *Mater. Chem. Phys.* **1987**, *18*, 287–294.
- (17) Li, R.; Zhen, Q.; Drache, M.; Rubbens, A.; Estournes, C.; Vannier, R. N. Synthesis and ion conductivity of (Bi₂O₃)_{0.75}(Dy₂O₃)_{0.25} ceramics with grain sizes from the nano to the micro scale. *Solid State Ionics* **2011**, *198*, 6–15.
- (18) Takahashi, T. *High Conductivity Solid Ionic Conductors: Recent Trends and Applications*; World Scientific: Nagoya, 1989.
- (19) Dordor, P. J.; Tanaka, J.; Watanabe, A. Electrical Characterization of Phase-Transition in Yttrium doped Bismuth Oxide, Bi_{1.55}Y_{0.45}O₃. *Solid State Ionics* **1987**, *25*, 177–181.
- (20) Lee, K. T.; Lidie, A. A.; Jeon, S. Y.; Hitz, G. T.; Song, S. J.; Wachsman, E. D. Highly functional nano-scale stabilized bismuth oxides via reverse strike co-precipitation for solid oxide fuel cells. *J. Mater. Chem. A* **2013**, *1*, 6199–6207.
- (21) Macdonald, J. R. *Impedance Spectroscopy*; Wiley: New York, 1987.
- (22) Wang, L. S.; Barnett, S. A. Deposition and Properties of Yttria-Stabilized Bi₂O₃ Thin-Films Using Reactive Direct-Current Magnetron Cosputtering. *J. Electrochem. Soc.* **1992**, *139*, 2567–2572.
- (23) Souza, E. C. C.; Chueh, W. C.; Jung, W.; Muccillo, E. N. S.; Haile, S. M. Ionic and Electronic Conductivity of Nanostructured, Samaria-Doped Ceria. *J. Electrochem. Soc.* **2012**, *159*, K127–K135.
- (24) Sannes, N. M.; Tompsett, G. A.; Nafe, H.; Aldinger, F. Bismuth based oxide electrolytes - Structure and ionic conductivity. *J. Eur. Ceram. Soc.* **1999**, *19*, 1801–1826.
- (25) Jiang, N. X.; Wachsman, E. D. Structural stability and conductivity of phase-stabilized cubic bismuth oxides. *J. Am. Ceram. Soc.* **1999**, *82*, 3057–3064.
- (26) Shuk, P.; Wiemhofer, H. D.; Guth, U.; Gopel, W.; Greenblatt, M. Oxide ion conducting solid electrolytes based on Bi₂O₃. *Solid State Ionics* **1996**, *89*, 179–196.
- (27) Sanna, S.; Esposito, V.; Graves, C.; Hjelm, J.; Andreasen, J. W.; Pryds, N. Structural instability and electrical properties in epitaxial Er₂O₃-stabilized Bi₂O₃ thin films. *Solid State Ionics* **2014**, *266*, 13–18.
- (28) Sun, J.-W.; Kang, L.-S.; Kim, J.-S.; Joung, M.-R.; Nahm, S.; Seong, T.-G.; Kang, C.-Y.; Kim, J.-H. Structural and electrical properties of Bi₂O₃-Nb₂O₅ thin films grown at low temperatures by pulsed laser deposition. *Acta Mater.* **2011**, *59*, 5434–5439.
- (29) Göbel, M. C.; Gregori, G.; Guo, X. X.; Maier, J. Boundary effects on the electrical conductivity of pure and doped cerium oxide thin films. *Phys. Chem. Chem. Phys.* **2010**, *12*, 14351–14361.
- (30) Lee, H. B.; Prinz, F. B.; Cai, W. Atomistic simulations of grain boundary segregation in nanocrystalline yttria-stabilized zirconia and gadolinia-doped ceria solid oxide electrolytes. *Acta Mater.* **2013**, *61*, 3872–3887.
- (31) Nakagawa, T.; Sakaguchi, I.; Shibata, N.; Matsunaga, K.; Yamamoto, T.; Haneda, H.; Ikuhara, Y. Oxygen diffusion blocking of single grain boundary in yttria-doped zirconia bicrystals. *J. Mater. Sci.* **2005**, *40*, 3185–3190.
- (32) Guo, X.; Maier, J. Grain boundary blocking effect in zirconia: A Schottky barrier analysis. *J. Electrochem. Soc.* **2001**, *148*, E121–E126.
- (33) Buban, J. P.; Matsunaga, K.; Chen, J.; Shibata, N.; Ching, W. Y.; Yamamoto, T.; Ikuhara, Y. Grain boundary strengthening in alumina by rare earth impurities. *Science* **2006**, *311*, 212–215.
- (34) Chung, S. Y.; Choi, S. Y.; Yoon, H. I.; Kim, H. S.; Bae, H. B. Subsurface Space-Charge Dopant Segregation to Compensate Surface Excess Charge in a Perovskite Oxide. *Angew. Chem., Int. Ed.* **2016**, *55*, 9680–9684.
- (35) Arora, G.; Aidhy, D. S. Segregation and binding energetics at grain boundaries in fluorite oxides. *J. Mater. Chem. A* **2017**, *5*, 4026–4035.
- (36) Hsieh, C. Y.; Fung, K. Z. Crystal structure and electrical conductivity of cubic fluorite-based (YO_{1.5})_x(WO₃)_{0.15}(BiO_{1.5})_{0.85-x} (0 ≤ x ≤ 0.4) solid solutions. *J. Solid State Electrochem.* **2009**, *13*, 951–957.
- (37) Ikeda, J. A. S.; Chiang, Y. M. Space-Charge Segregation at Grain-Boundaries in Titanium-Dioxide .1. Relationship between

Lattice Defect Chemistry and Space-Charge Potential. *J. Am. Ceram. Soc.* **1993**, *76*, 2437–2446.

(38) Rahaman, M. N. *Ceramic Processing and Sintering*, 2nd ed.; CRC Press: New York, 1995.

(39) Jung, D. W.; Nino, J. C.; Duncan, K. L.; Bishop, S. R.; Wachsmann, E. D. Enhanced long-term stability of bismuth oxide-based electrolytes for operation at 500 °C. *Ionics* **2010**, *16*, 97–103.